Climate Dynamics (2005)
DOI 10.1007/s00382-005-0005-8

**Filip Lefebre · Xavier Fettweis · Hubert Gallée
Jean-Pascal Van Ypersele · Philippe Marbaix
Wouter Greuell · Pierluigi Calanca**

Evaluation of a high-resolution regional climate simulation over Greenland

Received: 2 September 2004 / Accepted: 12 January 2005

Abstract A simulation of the 1991 summer has been performed over south Greenland with a coupled atmosphere–snow regional climate model (RCM) forced by the ECMWF re-analysis. The simulation is evaluated with in-situ coastal and ice-sheet atmospheric and glaciological observations. Modelled air temperature, specific humidity, wind speed and radiative fluxes are in good agreement with the available observations, although uncertainties in the radiative transfer scheme need further investigation to improve the model's performance. In the sub-surface snow-ice model, surface albedo is calculated from the simulated snow grain shape and size, snow depth, meltwater accumulation, cloudiness and ice albedo. The use of snow metamorphism processes allows a realistic modelling of the temporal variations in the surface albedo during both melting periods and accumulation events. Concerning the surface albedo, the main finding is that an accurate albedo simulation during the melting season strongly depends on a proper initialization of the surface conditions which mainly result from winter accumulation processes. Furthermore, in a sensitivity experiment with a constant 0.8 albedo over the whole ice sheet, the average amount of melt decreased by more than 60%, which highlights the importance of a correctly simulated surface albedo. The use of this coupled atmosphere–snow RCM offers new perspectives in the study of the Greenland surface mass balance due to the represented feedback between the surface climate and the surface albedo, which is the most sensitive parameter in energy-balance-based ablation calculations.

F. Lefebre (✉) · X. Fettweis · J.-P. Van Ypersele · P. Marbaix
Institut d'Astronomie et de Géophysique G. Lemaître,
Université catholique de Louvain, Louvain-la-Neuve, Belgium

F. Lefebre
Vito—Flemish Institute for Technological Research, Integral Environmental Studies, Boeretang 200, 2400 Mol, Belgium
E-mail: Filip.Lefebre@vito.be
Tel.: +32-14-336847

H. Gallée
Laboratoire de Glaciologie et de Géophysique de l'Environnement, Grenoble, France

W. Greuell
Institute for Marine and Atmospheric Research,
Utrecht University, Utrecht, The Netherlands

P. Calanca
Swiss Federal Research Station for Agroecology and Agriculture,
Zurich, Switzerland

1 Introduction

One of the unknowns of the projected global warming due to anthropogenic forcing is the expected mean sea-level rise. The contribution of each individual component, i.e., the ocean's thermal expansion as well as the mass budgets of Antarctica, Greenland and the continental small ice caps and glaciers, must be known (Houghton et al. 2001).

Experimental campaigns such as EGIG 1959 and 1967 (Ambach 1988), ETH-Camp (Ohmura et al. 1992), GIMEX (Oerlemans and Vugts 1993), KABEG (Heinemann 1999) and PARCA (Thomas et al. 2001) give local instantaneous information of the surface mass balance but it is hazardous to estimate the total Greenland surface mass balance from these measurements because of their limited spatial and/or temporal resolution.

In contrast with these measurements, numerical models offer the possibility to evaluate past, present and future changes in the Greenland mass balance. Numerical models also allow the separation and quantification of each individual process contributing to the ice sheet's mass balance.

Van de Wal and Oerlemans (1994) were the first to calculate the Greenland surface mass balance by means of an energy-balance model but made use of simple parameterizations for the incoming short and longwave radiation fluxes. Also, the turbulent energy fluxes were

based on simple linear relationships and no distinction between the sensible and latent heat flux was made.

Global circulation models (GCMs) also explicitly calculate the surface energy balance and are suited for climate change experiments. However, their major weakness is their rather coarse horizontal resolution. They are unable to represent, for example the Greenland ablation zone, which ranges from a few kilometers in the south-east to 100 km at its largest in west Greenland. Also, the ice sheet topography is not exactly represented and leads to important errors in the amount of cloudiness, precipitation and ablation. Ohmura et al. (1996) showed the high sensitivity to horizontal resolution of the simulated precipitation field. Furthermore, Hanna and Valdes (2001) analyzed the European Centre for Medium-Range Weather Forecasts (ECMWF) ERA-15 re-analysis surface climate data for the period 1979–1998 in detail and found that surface albedo and cloud errors need to be rectified if the analysis are used effectively to drive energy balance models for Greenland ablation calculations.

Another problem is that most GCMs do not include physically based surface albedo parameterizations nor do they include ice-sheet-specific processes such as refreezing of meltwater, which is of major importance in the Greenland higher ablation and percolation zone (Pfeffer et al. 1991). It is of capital importance to correctly simulate the surface albedo since a small albedo error may induce important errors in the simulated surface net radiation balance, which is the major source of energy to heat and melt snow and ice. Nolin and Stroeve (1997) showed that even in areas that experience little or no melt, important surface albedo decreases of 10–20% are common. These reductions are found to be related to slow increases in snow grain size.

A way to refine and correct GCM predictions of the Greenland surface mass balance is to nest a regional climate model (RCM) within GCM-generated atmospheric fields. The RCM can be run at a higher resolution, thereby more correctly representing the topography of the steep Greenland ice-sheet margins, which improves the simulated atmospheric fields (Georgi et al. 1999) that force the surface mass balance.

Cassano et al. (2001) presented an evaluation of an annual atmospheric simulation over Greenland with the Polar MM5 model. It should be stressed that their simulation was compiled from a series of short-duration (48 h), forecast-mode simulations. From these 48-h simulations, only the last 24 h are used. In the Polar MM5, the Greenland ice-sheet surface is represented by a diffusive multi-layer surface model with fixed surface properties. In particular, the use of a fixed surface albedo (0.8) can lead to large errors in the simulated net radiation budget over melting surfaces during the summer.

In this paper, we will present an evaluation of a coupled model run in which a high-resolution (20 km) atmospheric RCM is coupled with a physically based snow-ice model. Specific surface processes such as melting, percolation and refreezing of meltwater as well as snow grain metamorphism processes and closely related snow albedo variations are taken into account. The coupled RCM will be applied over south Greenland during the 1991 ablation season. It is nested into the ECMWF ERA-15 re-analysis with a single initialization procedure at the start of the simulation. In a first attempt, we will focus on the summer season and the accuracy of the surface albedo simulation. The use of re-analyzed forcing fields instead of present climate GCM output minimizes the errors that could be due to wrong input data. It also enables us to compare the model output with in-situ observations. This work is part of a long-term research project to better estimate the Greenland climate and surface mass balance (Gallée et al. 1995; Gallée and Duynkerke 1997; Lefebre et al. (2003). In the next section, a brief description of the coupled atmosphere–snow RCM is given. Afterwards, the simulation is described and evaluated by comparison with near-surface atmospheric and mass balance measurements. In particular, the simulated surface albedo will be compared with observations from three locations on the ice sheet. The reference experiment will also be compared with a sensitivity experiment in which the surface albedo is kept constant at 0.8 over the ice sheet.

2 Coupled atmosphere–snow RCM

2.1 General description

The coupled atmosphere–snow RCM used is Modèle Atmosphérique Régional (MAR). The atmospheric part of MAR is fully described in Gallée and Schayes (1994) and Gallée (1995). MAR is a hydrostatic primitive equation model in which the vertical coordinate is the normalized pressure

$$\sigma = \frac{p - p_t}{p_s - p_t}, \tag{1}$$

where p, p_t and p_s being the pressure, the constant model top pressure and the surface pressure, respectively. MAR was originally developed for process studies in the polar regions but is now besides Antarctica (Naithani et al. 2002) also applied over Europe for nested climatic studies (Marbaix 2000; Brasseur et al. 2002). The lateral boundary nudging treatment consists of a buffer zone (width of 5 points) involving ''Newtonian'' and ''diffusive'' relaxation terms. Lateral boundary conditions are updated every 6 h and a linear interpolation is made in between (Davies 1983; Marbaix et al. 2003).

Sea surface temperatures are prescribed from ECMWF re-analysis. Sea ice is not modelled explicitly but its distribution is deduced from ECMWF sea surface temperatures. Inside the ECMWF re-analysis system, satellite observations are used to define the actual sea-ice distribution (Nomura 1995). Open water and sea ice have an albedo of 0.07 and 0.55, respectively. A band of

tundra points borders the inland ice sheet. In case of a snow-free tundra surface, the force-restore surface model of Deardorff (1978) with a soil thermal conductivity of 0.65 W m^{-1} K^{-1} and an albedo of 0.20 is used to predict the tundra surface temperature. When snow covers the tundra soil, the snow model is used (see below).

2.2 Snow and ice model

The snow model is described in detail in Gallée and Duynkerke (1997) and Gallée et al. (2001). It is validated for a site on the Greenland ice sheet (ETH-Camp, west Greenland, 1150 m a.s.l.) in Lefebre et al. (2003).

In the multi-layered thermodynamic 1D snow model, snow metamorphism processes are represented by the CROCUS snow metamorphism laws (Brun et al. 1992). The latter allow us, in combination with the detailed meltwater budget representation, to represent the evolution of the snow grain characteristics (shape and size) and its albedo.

Afterwards, the surface albedo is calculated from (1) the snow albedo, (2) the depth of the snow pack upon the ice or the tundra, (3) the accumulated meltwater (over the ice sheet only) and (4) the albedo of the underlying ice or tundra.

During off-line (forced with observations) simulations at ETH-Camp (west Greenland), the simulated surface albedo and the simulated surface mass balance were found to be in good agreement with the observations (Lefebre et al. 2003).

In the present article, the same snow model configuration as the one used for the validation is used with two modifications. The first change deals with the influence of atmospheric cloudiness on the surface albedo. Clouds tend to increase the proportion of the visible part of the solar radiation spectrum, modifying the incident solar radiation spectrum. This leads to a small increase of about 0.05 in the broadband surface albedo (Key et al. 2001). The coupling between the atmospheric part of MAR and its snow model uses a fixed solar radiation spectrum with the simulated broadband solar incident radiation flux. Therefore, an additional term in the surface albedo calculation has been added as in Greuell and Konzelmann (1994) to account for the small increase in surface albedo (up to 0.05) due to clouds.

Secondly, compared to the validated version, the density and grain size and shape for fresh snow are not calculated with the original CROCUS fresh snowfall parameters (dendricity, sphericity and density). In Lefebre et al. (2003), the original CROCUS fresh snow fall parameters proved to be adequate for ETH-Camp summer snowfalls. This is due to the location of the site, which is rather close (40 km) to the ice-sheet margin, and the occurrence of abundant surface melt. The latter rapidly transforms freshly fallen dendritic snow grains into round snow grains. In the present simulations, the fresh snow parameters ought to be valid not only in the Greenland ablation zone but also for the rest of the Greenland ice sheet, which also includes the ice-sheet dry snow zone where no melt occurs.

Therefore, fresh snow is characterized by a snow density of 300 kg m^{-3} and by round, 0.3-mm large spherical snow grains, in agreement with surface snow observations in the dry snow zone (Morris et al. 1997).

2.3 Model setup

The simulation starts on the first of May 1991 and lasts until the end of August, i.e., 123 days, which corresponds with the major melting period over the Greenland ice sheet. Mass balance observations at ETH-Camp during the 1991 field season revealed that the melting season stopped around mid-August.

The integration domain encompasses the southern part of Greenland and its neighboring waters (Fig. 1). MAR fine-grid topography and soil type for Greenland

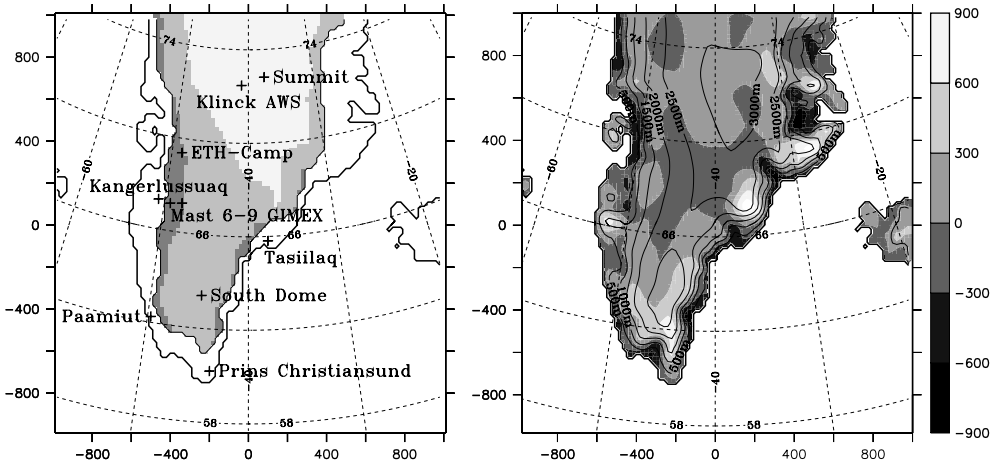

Fig. 1 *Left* The prescribed distribution of MAR mass balance zones on the Greenland ice sheet and the major locations referred to in the text. From *black* to *light gray* over the ice sheet: ice-sheet ablation zone, percolation zone and dry snow zone. The model ablation zone delineation is specified and taken from Reeh (1991). *Right* MAR surface height (*isolines*) and the difference (*shades of gray*) between MAR and ECMWF model surface height

are taken from the Ekholm (1996) Greenland topography and land masks. The size of the domain is 2,000 km × 2,000 km with a high horizontal resolution of 20 km in order to represent the ice-sheet ablation zone and the succession of the different mass balance zones. Denby (2001) examined the sensitivity of turbulent fluxes and katabatic wind speed maximums to the horizontal resolution. A resolution of 20 km proved to be a good compromise. Wind speed maxima only slightly increased at 10 km resolution. Therefore, a resolution of 20 km enables a correct representation of the katabatic winds and henceforth of the turbulent heat fluxes due to the mixing of warmer air from above with the cold air in the vicinity of the ice sheet's surface. Although a higher resolution would still be recommendable for some very steep locations (for example in east Greenland), previous regional atmospheric simulations with complete 3D models (e.g., Cassano et al. 2001; Bromwich et al. 2001b) never used resolutions finer than 40 km. Computing time is still a limiting factor in regional climatic simulations.

Strong vertical gradients of wind speed and temperature are found close to the surface of the Greenland ice sheet. Therefore, the lowest atmospheric model level has been put at 2 m above the surface. The next four levels are situated at 4, 8, 16 and 32 m above the surface. The model has been initialized once. The lateral boundaries are updated every 6 h with the ECMWF ERA-15 reanalysis for temperature, specific humidity, wind components and surface pressure. Linear interpolation in time is made in between.

2.4 Initialization

Atmospheric wind components, air temperature and specific humidity as well as the surface temperatures and deep-soil tundra temperatures are initialized from the ECMWF ERA-15 re-analysis. Ideally, we should spin-up the snow model separately during a long-term period to obtain equilibrated snow and ice initial temperature and density fields. For our simulations, we have in a first attempt, prescribed these initial fields. In particular over the ice sheet, the snow and ice initial temperatures are initialized by linear interpolation between the ECMWF ERA-15 surface temperature and the climatological deep snow and ice temperature (T_{ann}). The latter was taken from Reeh (1991), who derived a parameterization based on long-term ice-sheet temperature records for the 1951–1961 period. This parameterization, or with slightly different parameters, is also used in thermodynamic ice-sheet models of the Greenland ice sheet as an approximation of the annual average surface temperature (see, e.g., Huybrechts et al. 1991; Ritz et al. 1997):

$$T_{\mathrm{ann}}\,(\mathrm{in}\,^{\circ}\mathrm{C}) = 48.38 - 0.007924E - 0.7512L \qquad (2)$$

with E the surface elevation (m) and L the latitude (°N).

The dry snow zone has been delineated as the area with an annual mean temperature of less than −25°C (Benson 1962). The model ablation zone delineation is taken from Reeh (1991). In the model ablation zone, the 1990–1991 winter precipitated snow from Bromwich et al. (2001a) is laid on top of a 20-m thick prescribed ice pack. Because of lack of reliable data, we neglect the impact of snow drift, evaporation and sublimation. This can eventually lead to an overestimation of more than 10% of the snow pack height according to Box and Steffen (2001). A typical surface snow density of 300 kg m^{-3} has been chosen (Morris et al. 1997). In the area between the ablation zone and the dry snow zone (denoted percolation zone), the snow density has been put equal to 500 kg m^{-3} for the lowest 20 m of the snow pack. On top of it, as in the ablation zone, the Bromwich et al. (2001a) 1990–1991 winter snow fall has been added with a density of 300 kg m^{-3}. In the dry snow zone, the snow density between the bottom of the snow model at 20-m depth and the surface snow has been calculated with the empirical density-depth relation from Schytt (1958):

$$\rho = \rho_{\mathrm{i}} - (\rho_{\mathrm{i}} - \rho_{\mathrm{s}})\exp(-Cz), \qquad (3)$$

where ρ is density at depth z, ρ_{i} the density of ice (920 kg m^{-3}), ρ_{s} the density of surface snow (300 kg m^{-3}), and C is a constant which has been set to $1.9/z_{\mathrm{t}}$, where z_{t} is the depth of the firn-ice transition. z_{t} varies with the accumulation rate and surface climate, and has been put at 70 m, a typical value for Greenland (Paterson 1994).

Lastly, the tundra area has also been covered with the winter 1990–1991 snow pack since the start of the simulation takes place on the first of May 1991. Table 1 and Fig. 1 summarize the details of the snow and ice initial state.

Table 1 Snow–ice model initial state characteristics

Model mass balance zone	Vertical structure	Snow-ice model density (kg m^{-3})	Snow grain size (mm)
Dry snow zone	20 m of snow	Eq. 3	0.3
Percolation zone	20 m of snow + Bromwich (2001a) 1990–1991 winter snow	500 + 300	0.3 (0.3)[a]
Ablation zone	20 m ice + Bromwich (2001a) 1990–1991 winter snow	920 + 300	(0.3)[a]
Tundra area	Bromwich (2001a) 1990–1991 winter snow	300	0.3

[a]Values in parenthesis are from Bromwich (2001a) 1990–1991 winter snow

3 Evaluation of the model results

Model grid point results are instantaneous values averaged for the whole grid cell area. Comparing those values with local observations must be done carefully. The model grid cell closest to the observation site does not necessarily have the same elevation as the observation site. Moreover, sub-grid topography roughness and local surface variability (surface albedo, surface emissivity and soil heat capacity) can locally influence the air motion and thermodynamic air characteristics. Higher up the ice sheet, in the dry snow zone, these effects are likely less important since the surface is more homogeneous and flat. However, in the lower ablation zone and in the tundra area these effects may be very important. For example, measurements at Kangerlussuaq (67.01°N and 50.70°W) in the tundra area on west Greenland are influenced by the local conditions since the weather station is situated near the local airport where the surface is covered by asphalt. Table 2 gives an overview of the locations used in the comparison. Data from one coastal weather station operated by the Danish Meteorological Institute and from four on-ice sites have been used. One of the ice-sheet stations is situated in the dry snow area (AWS-Klinck), two others are located close to the long-term equilibrium line (ETH-Camp and GIMEX-M9) and the last one (GIMEX-M6) is in the ablation zone.

3.1 Model evaluation at ETH-Camp

ETH-Camp is located some 40 km far from the ice-sheet margin, close to the long-term equilibrium line. In the model, it is located in a grid cell inside the ice-sheet ablation zone neighboring the equilibrium line altitude. A description of the 1991 intensive measurement campaign at ETH-Camp is given in Ohmura et al. (1992). In this section, we will compare in detail MAR modelled and observed variables at ETH-Camp for the period between 9 May and 30 August 1991 (see Fig. 2 and Table 3). This is done in order to explain some of the strong points and deficiencies related to the coupling of the atmospheric model with the snow model. Also, the ERA-15 fields interpolated on the MAR grid have been added in the comparison. ERA-15 fields are linearly interpolated from the 'reduced' Gaussian grid which was used to construct the ERA-15 re-analysis. At 70°N, the ERA-15 west-east resolution is 2.8125°, which corresponds to a horizontal resolution of about 106 km. This coarse resolution makes comparisons with point observations difficult. Interpolated ERA-15 values close to the ice-sheet margin will be influenced by the presence of the tundra area.

During the whole period, MAR simulated surface boundary layer (SBL) temperatures are in close agreement with the observations. On the contrary, the ERA-15 SBL temperatures are overestimated during the month of July. Furthermore, the ERA-15 humidity and wind speed in the SBL are underestimated during that period, while the same variables in MAR are in closer agreement with the observations (see also Table 3).

These deficiencies are probably caused by a coarse representation of the ECMWF planetary boundary layer. First, the larger height of the first vertical layer in the ECMWF model (roughly 40 m) compared to that of the MAR model (roughly 2 m) induces errors in the representation of the katabatic vertical structure. In fact, the vertical profile of the persistent katabatic wind speed exhibits a low-level wind speed maximum that is not resolved in the ECMWF model. The katabatic winds are too-weak in the ECMWF model and this is responsible for an underestimation of the downward sensible (upward latent) surface heat fluxes, leading to an additional overestimation of the SBL temperature and a subsequent too weak katabatic wind forcing. Note also that the surface slope is not well represented in ERA-15 because of its coarse horizontal resolution. Besides the resolution issue, simulated winds are also underestimated due to the first-order turbulence closure schemes inside the ECMWF ERA-15 model (Gibson et al. 1999) that are known not to be adequate during stable conditions (Denby 2001).

In addition to Fig. 2 which shows daily average values during the whole simulation period, Fig. 3 demonstrates MAR ability to correctly simulate the daily cycle for the most important near-surface atmospheric parameters during a short period (June). The weather encountered during this month can be divided into two distinct periods. Before the 16th of June, the weather was characterized by a high-pressure synoptic situation that led to clear skies with large daily cycles in temperature, humidity and wind speed. Afterwards, the surface pressure dropped until the end of the month and clouds appeared, which lead to damped daily cycles of these atmospheric variables.

Table 2 Geographical positions and elevations of the locations used in the comparison

Site	Latitude (°N)	Longitude (°W)	Observed elevation (m)	MAR elevation (m)	ERA elevation (m)
ETH-Camp	69.57	49.29	1155	1153	1266
GIMEX-M6	67.06	49.35	1028	1027	1143
GIMEX-M9	67.03	48.28	1520	1597	1607
AWS-Klinck	72.31	40.48	3105	3080	3019
Kangerlussuaq	67.01	50.70	50	340	692

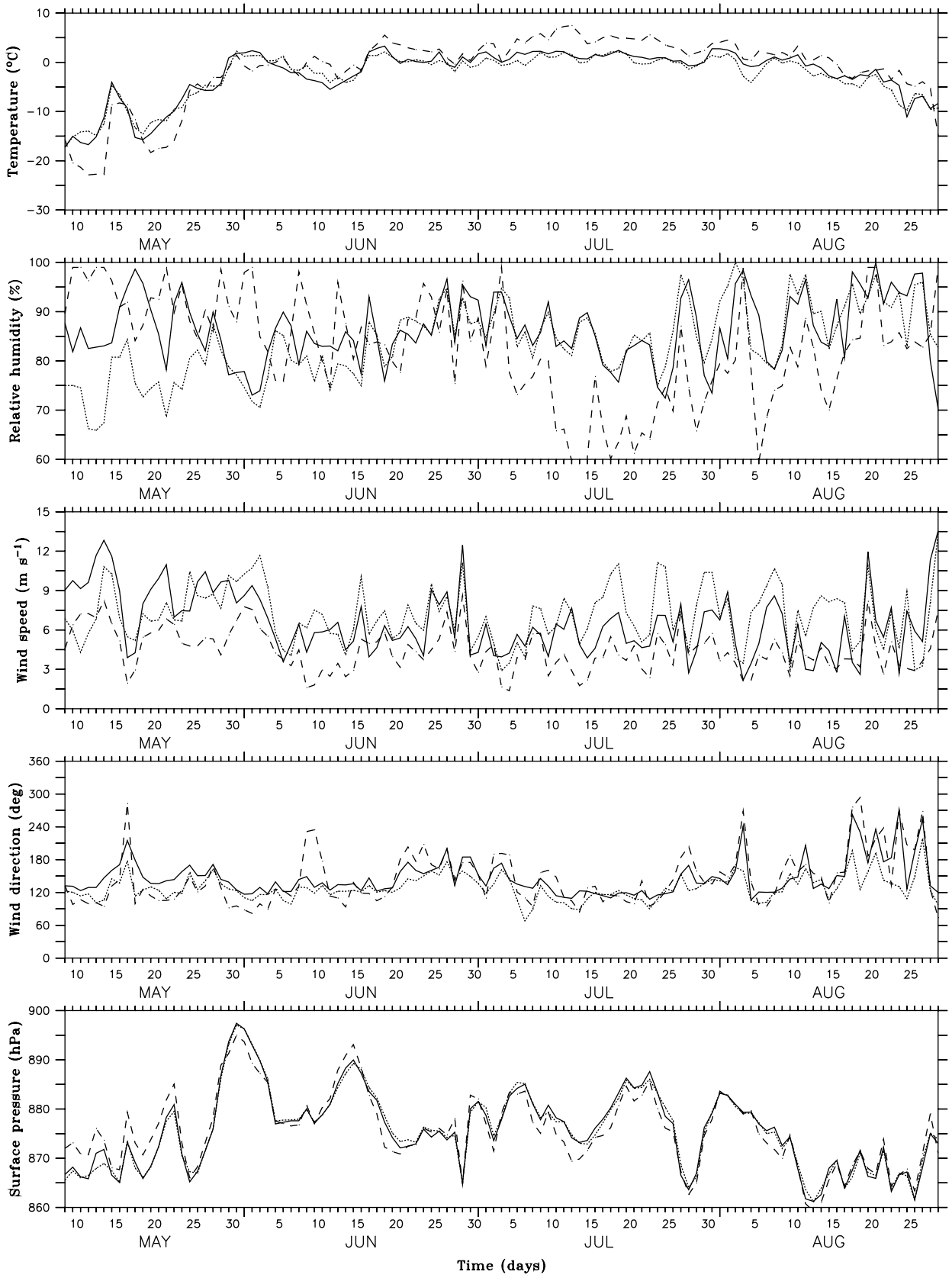

Fig. 2 Comparison between observed (*dotted*), MAR (*solid*) and ECMWF (*dashed*) modelled air temperature, relative humidity, wind speed, wind direction and surface pressure (daily average values) at ETH-Camp during the whole simulation

Table 3 Statistics at ETH-Camp during the summer of 1991 based on 6-hourly values for the period from the 9th of May until the 30th of August

Variable	Obs. mean	MAR bias	ERA bias	MAR rmse	ERA rmse	MAR corr	ERA corr
Air temperature (°C)	−2.77	+0.39	+1.42	1.99	4.16	0.94	0.86
Relative humidity (%)	83.86	+1.58	−2.12	7.43	14.98	0.63	0.01
Wind speed (m s^{-1})	7.17	−0.60	−2.70	2.70	3.56	0.60	0.54
Wind direction (°)	128.6	+18.0	+16.5	35.4	50.0	0.66	0.59
Surface pressure (hPa)	875.8	−0.04	+0.00	1.21	2.69	0.99	0.94
Surface albedo (−)	0.75	−0.05	−0.25	0.11	0.26	0.53	0.49

The surface energy balance, which drives the surface mass balance, is largely controlled by the radiative fluxes and the surface albedo and to a lesser extent by the turbulent fluxes (van den Broeke et al. 1994). Table 4 contains the observed averages, MAR bias and root mean square error for the radiative fluxes and this for the whole duration of intensive radiative measurements at ETH-camp (3 June until 18 August), for cloudy days and for clear-sky days.

MAR overestimates the amount of incoming solar radiation. This overestimation ($+26.5$ W m^{-2}) is somewhat compensated by an underestimation (-14.7 W m^{-2}) of the downward longwave radiation. Nevertheless, due to the high surface albedo for snow (about 75%), one has to conclude that the net radiation balance is still underestimated by about 8 W m^{-2}.

A comparison between cloudy and clear-sky conditions indicates that most of the errors are caused during cloudy conditions. This is also shown in Fig. 3, where the largest errors in the simulated downward longwave radiation occur during cloudy days, i.e., days with reduced solar downward radiation. In MAR, longwave radiation is calculated with the scheme of Morcrette (1984) that was designed for use in GCM models and that was also used during the calculation of the ERA-15 re-analysis. It was found by Morcrette (2002) that this version of the longwave scheme underestimates the downward infrared radiation at the surface. In addition, errors in the simulated cloud emissivities could further contribute to that negative bias. This problem will be corrected in the future by using the new ECMWF radiative transfer scheme (Morcrette 2002).

During the 1991 ETH-expedition, eddy-correlation measurements were made to evaluate the turbulent momentum and heat fluxes (Forrer and Rotach 1997). Data are only available during some periods of the ablation season. Therefore, we have compared the model results with observations, by means of scatter plots (Fig. 4).

Simulated friction velocities are in agreement with the observations for values lower than 0.3 ms^{-1} but show a positive bias at higher friction velocities. The agreement is acceptable for the sensible heat flux at 2 m (negative values represent downward heat fluxes), although MAR sometimes generates an upward sensible heat flux, contrary to the observations. It is difficult to make definite conclusions with only observations during some periods. Longer term continuous measurements are needed given the uncertainty of eddy-correlation turbulent flux measurements on sloping melting surfaces (Ohmura et al. 1992).

The surface albedo variations, observed at ETH-Camp between the start of the simulation and the end of July (Fig. 5), are solely caused by snow grain metamorphism processes because the surface was covered with a sufficiently thick snow pack so that the underlying ice does not interfere. During this period, it can be seen (middle graph in Fig. 5) that MAR modelled snow albedo closely follows the observed snow albedo variations, i.e., the lowering of the albedo due to growing snow grains when melt takes place and the abrupt increases due to snow falls simulated by the atmospheric model component. During these snow falls, fresh snow crystals with a high reflectance are deposited on top of the older larger snow grains. In particular, the timing of the onset and ending of the major melting period (3–26 July) coincides with the observations.

The disagreement at the beginning of August (1–10 August 1991) is caused by the modelled ice layers at the surface of the snow pack. These ice layers with a low albedo of 0.55 form because of the lower air temperatures in combination with the saturated snow pack. It should be noticed that at the same moment, slush was observed in the surroundings of the site. This suggests that the slush is probably not well treated by the snow model during refreezing conditions.

Afterwards (11–16 August 1991), due to the previously overamplified melt due to the underestimated surface albedo, the snow pack became too thin in comparison with the observations. Under these conditions, the model surface albedo is found to fluctuate between the high albedo coming from fresh snow and the low albedo (0.55) of the underlying ice. At the end of the simulation, simulated surface albedo values are again very close to the observations.

It should be stressed that a well-simulated surface albedo is only possible provided all conditions are fulfilled. In particular, the surface albedo model should not only be sufficiently detailed but also the initial conditions should be correct. For example, the simulated height of the snow pack upon the ice at ETH-Camp decreases slightly too fast (lower graph in Fig. 5), which causes the ice to appear too rapidly. This error can partly be explained by the somewhat underestimated mass balance of the initial snow pack caused by using a too small snow density at the beginning of the simula-

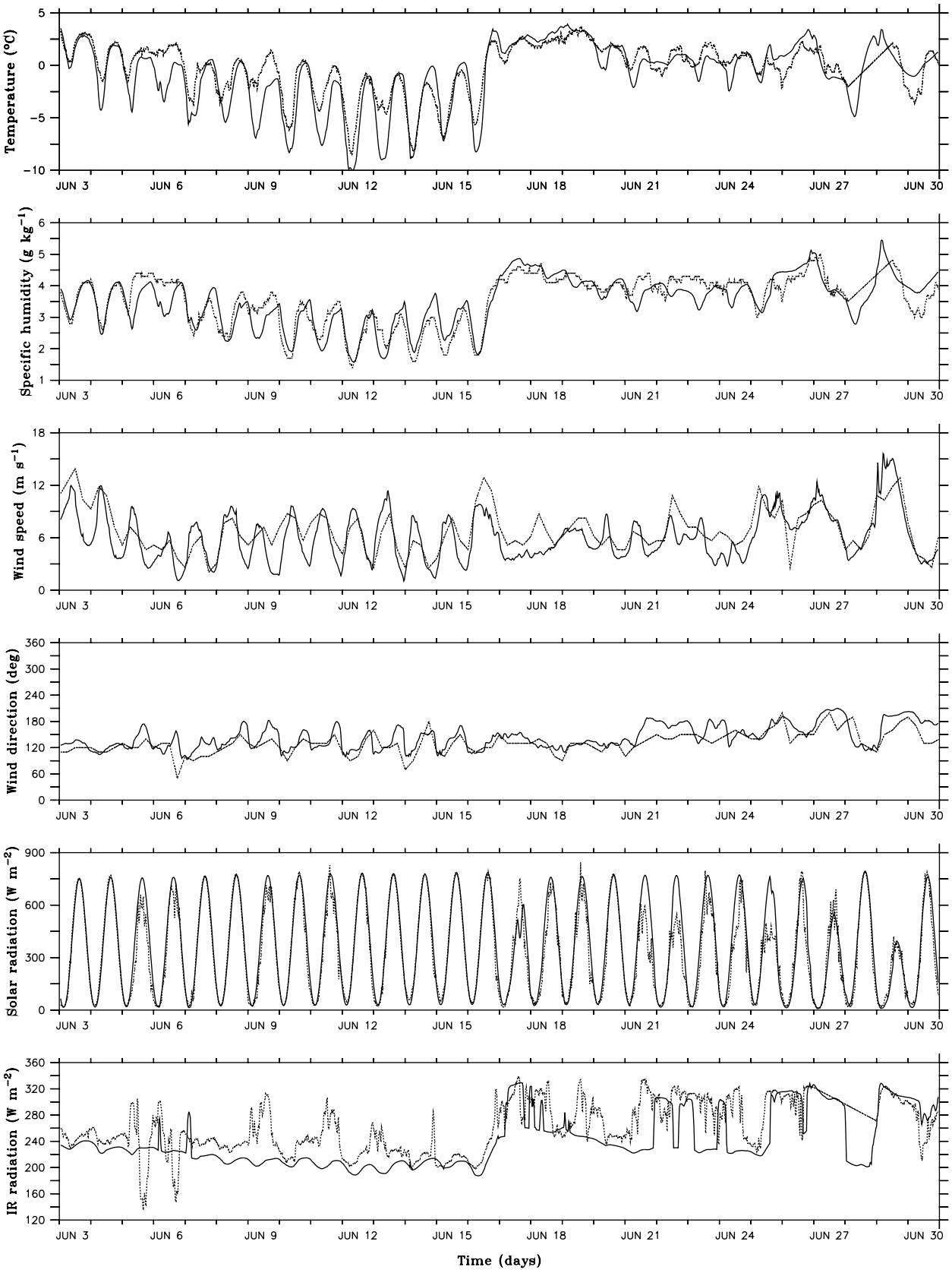

Fig. 3 Comparison between observed (*dotted*) and MAR modelled (*solid*) air temperature, air specific humidity, wind speed, wind direction, surface downward solar radiation and surface downward longwave radiation at ETH-Camp from half-hourly values during June 1991

Table 4 Statistics of the radiative fluxes (in W m^{-2}) at ETH-Camp during the summer of 1991 (3 June–18 August 1991) based on half-hourly values

Period	Variable	Observed mean	MAR bias	MAR rmse	MAR corr
3rd June ↔ 18th August	Solar ↓	301.11	+26.46	78.11	0.96
	IR ↓	261.51	−14.68	34.51	0.62
Cloudy	Solar ↓	222.79	+53.83	117.35	0.92
	IR ↓	302.81	−22.68	47.56	0.27
Clear sky	Solar ↓	340.11	+9.60	47.76	0.98
	IR ↓	240.95	−10.95	25.63	0.42

tion (300 kg m^{-3}). Indeed the initial thickness of the snow pack is comparable to the observed one. This has been verified by comparison with the observed snow pack mass balance at ETH-Camp at the start of the simulation.

The use of a snow albedo, which depends on the snow surface temperature as in the ERA-15 re-analysis project clearly induces a too small albedo when melt occurs. It can be seen that the ECMWF simulated surface albedo has already decreased to 0.4 at the beginning of June. This oversimplified albedo scheme has been updated in the actual ECMWF forecast model as well as in the production of the new ERA-40 re-analysis dataset (A. Beljaars, personal communication).

3.2 Model evaluation at the K-transect

During the GIMEX-91 experiment, seven weather stations, three on the tundra and four on the ice sheet, were placed along the K(angerlussuq)-transect at 67°N in west Greenland by the University of Utrecht and the Free University of Amsterdam. For more information about the experiment, the reader is referred to van den Broeke et al. (1994) who give a detailed description of the measurement campaign. We will use data from only two stations (GIMEX-M6 and GIMEX-M9) which are both located on the ice sheet. MAR's horizontal resolution (20 km) does not allow us to compare model output with measurements from the other locations situated at 2.2 km and 6.9 km from the ice-sheet border. GIMEX-M6 and GIMEX-M9 are located at approximately 40 km and 90 km from the ice-sheet border (Table 2).

Figures 6 and 7 compare MAR results with observations at GIMEX-M6 and GIMEX-M9, respectively. For GIMEX-M6, average hourly observations are available from 10 June until 24 July. At GIMEX-M9, half-hourly observations for the 5–24 July period have been obtained. Unfortunately, no turbulent flux measurements by eddy-correlation were available for these GIMEX sites.

Air temperature, air humidity, wind speed and wind direction are accurately simulated (Table 5). Solar downward radiation is overestimated, which confirms the results at ETH-Camp, although the solar radiation evolution (Fig. 6) shows that the cloud cover frequency is mostly correctly simulated by the model.

The overestimated surface albedo in MAR between 10th of June and 4th of July at GIMEX-M6 is due to the presence of an initial snow pack in the MAR model. Actually, at the beginning of the measurements, the ice-sheet surface at GIMEX-M6 was snow-free. After the modelled snow pack in MAR has melted away (4th July), the surface albedo agrees much better with the observed values.

At GIMEX-M9, the observed surface albedo between 5–24 July decreases from 0.80 to 0.65 (see Fig. 7). Surface melt occurred on every day only interrupted by one snowfall on 16 July. MAR modelled surface albedo also

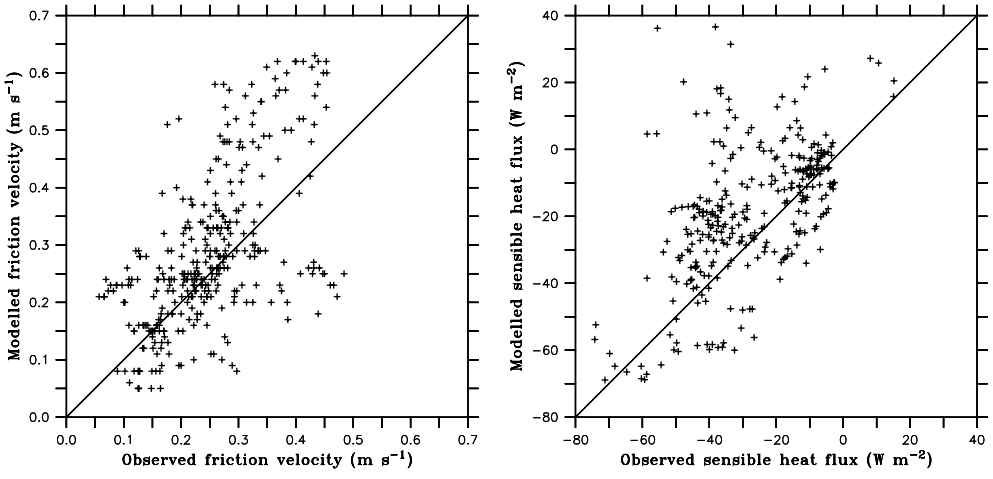

Fig. 4 Comparison between simulated and observed 2-m friction velocity (*left*) and sensible heat flux (*right*) at ETH-Camp during the summer of 1991

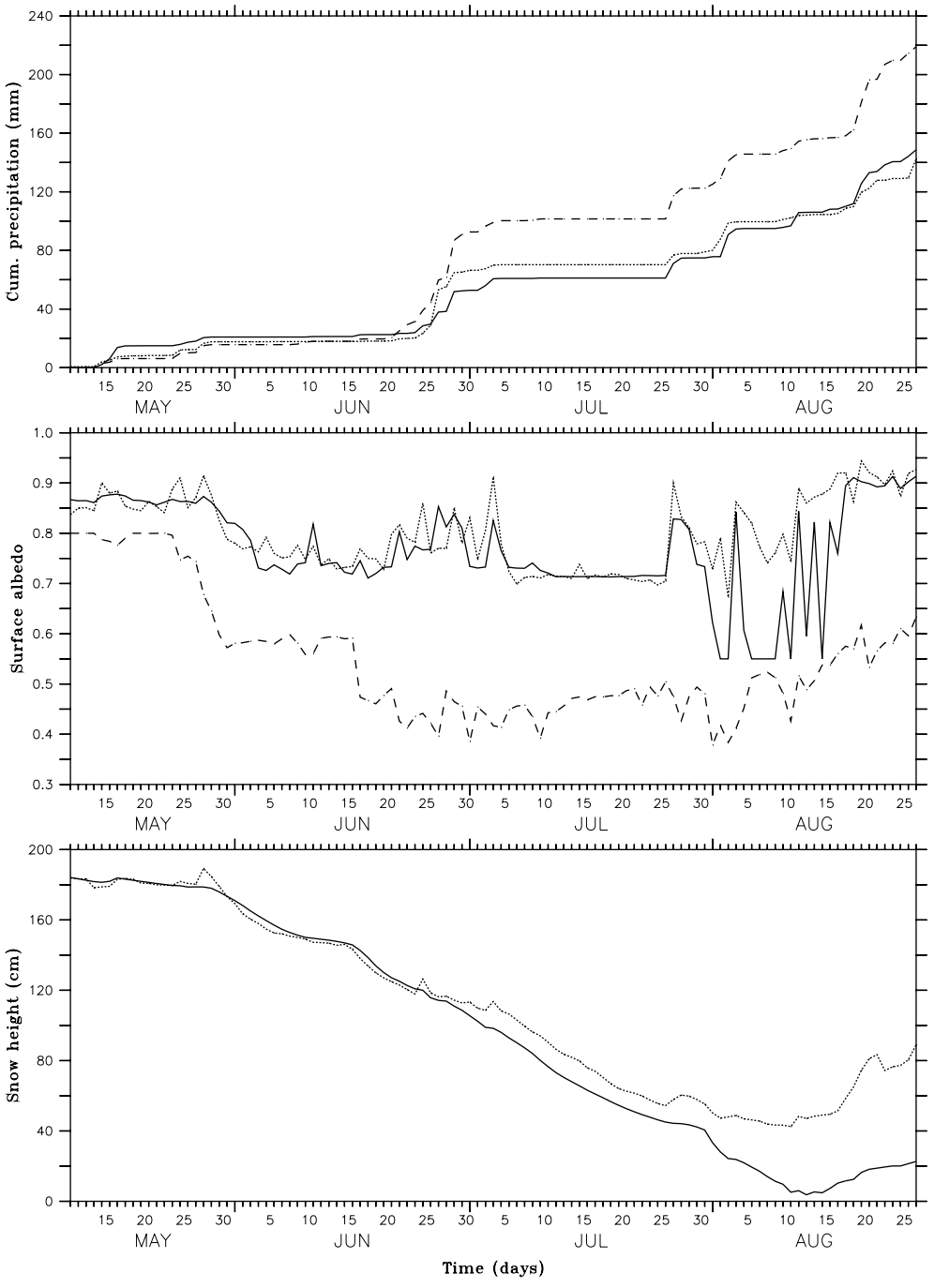

Fig. 5 *Top* Observed (*dotted*), MAR (*solid*) and ECMWF (*dashed*) cumulative precipitation at ETH-Camp; *Middle* same as above but for the surface albedo; *below* same as top graph but for the snow pack height

decreases due to growing snow grains. However, the modelled decrease is slightly too small. Ablation at GIMEX-M9 is characterized by a strong daily cycle with melt during the day and refreezing during the night (observed air temperatures fall below 0°C). This is successfully simulated by MAR.

The importance of an accurately simulated surface albedo clearly shows up when the results of a sensitivity experiment are analyzed in which the surface albedo is held constant at 0.8 over the whole sheet. This is shown for the GIMEX-M9 location (Fig. 7) where the use of a constant albedo clearly leads to stronger daily cycles because less heat from meltwater refreezing is available to act against the cooling during the night. Moreover, a too high surface albedo tends to increase the surface inversion, which increases the katabatic wind speed (visible between 22 and 27 July). But on average, the differences in the simulated atmospheric fields between both experiments are rather small. This is also the case at GIMEX-M6 and ETH-Camp (not shown here).

However, there is a significant impact on the simulated mass balance (Table 6). For example at GIMEX-M9 in the percolation zone, the initial snow height equals 141 cm above the ice. At the end of the

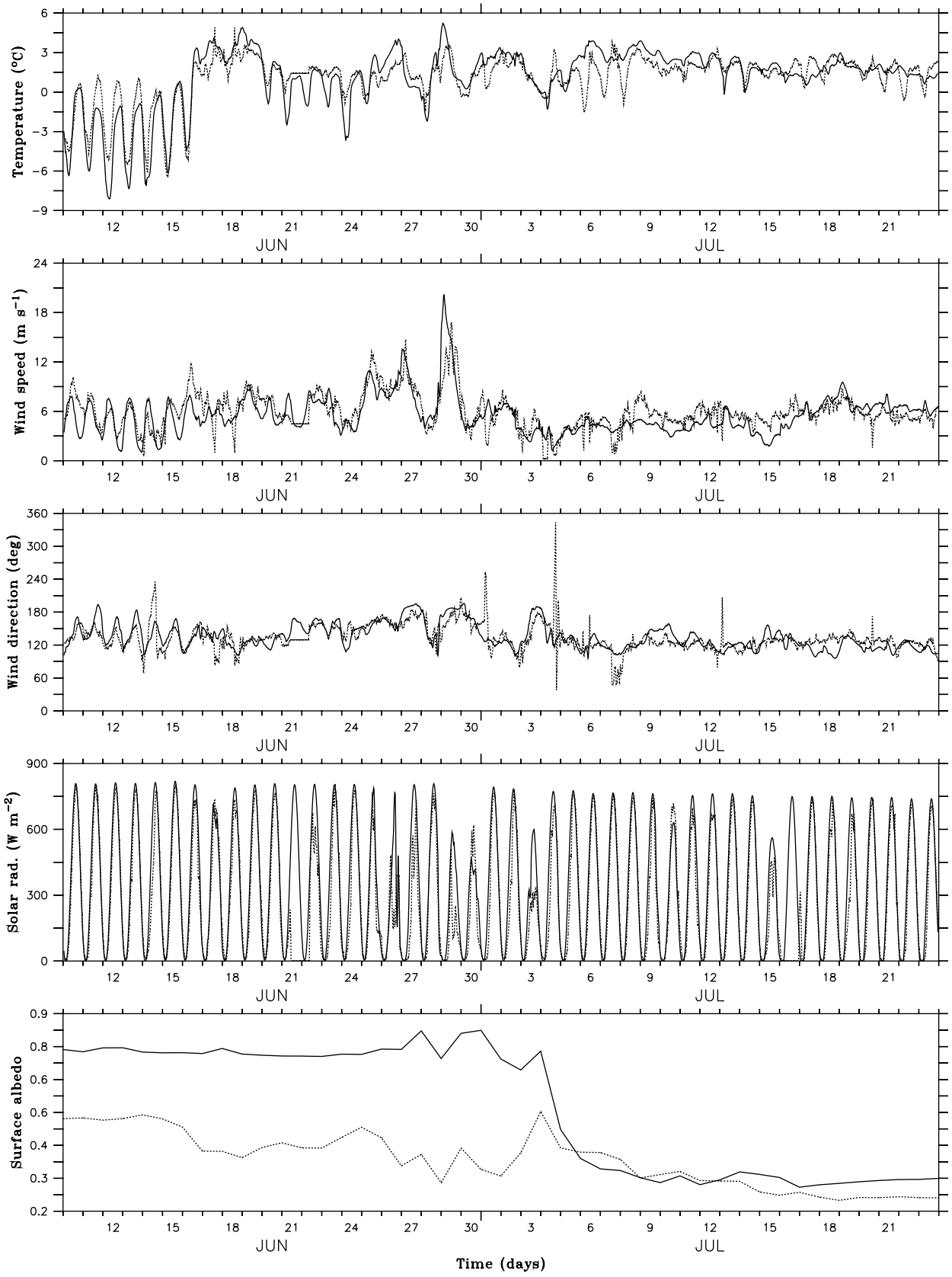

Fig. 6 MAR (*solid*) and observed (*dotted*) air temperature, wind speed, wind direction, surface downward solar radiation and surface albedo evolution at GIMEX-M6

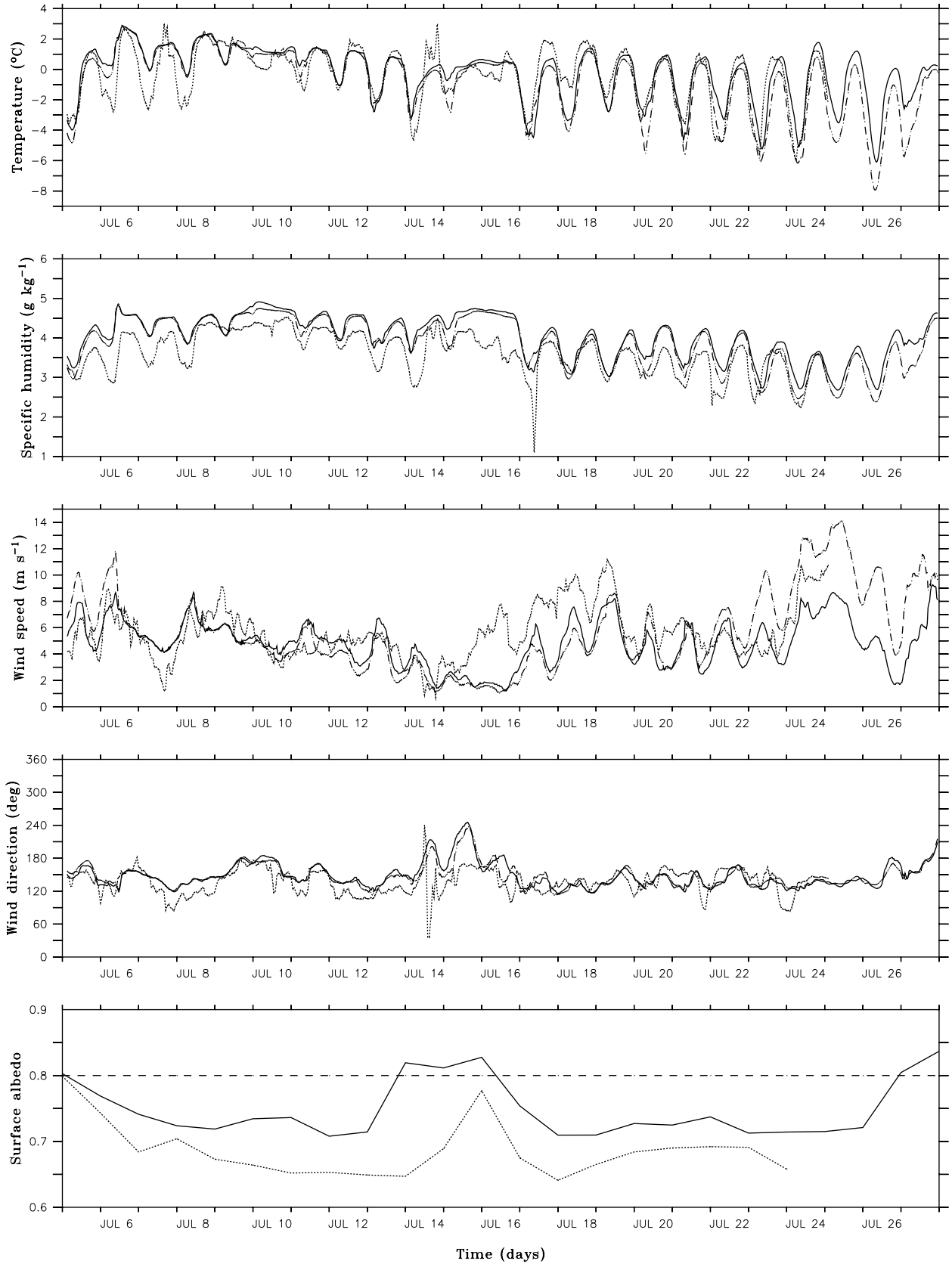

Fig. 7 As in Fig. 6 but at GIMEX-M9. The dashed curves are from a sensitivity experiment in which the surface albedo was held constant at 0.8 during the whole simulation over the whole ice sheet

Table 5 Statistics at GIMEX-M6 (hourly values) and GIMEX-M9 (half-hourly values) during the summer of 1991

Station	Variable	Obs mean	MAR bias	MAR rmse	MAR corr
GIMEX-M6 (10–24 July)	Air temperature (°C)	1.08	+0.07	1.18	0.86
	Wind speed (m s^{-1})	6.00	−0.37	1.76	0.72
	Wind direction (°)	133.40	−1.18	20.75	0.61
	Solar ↓ rad. (W m^{-2})	304.30	+44.37	99.50	0.95
	Surface albedo (−)	0.40	+0.16	0.21	0.76
GIMEX-M9 (5–24 July)	Air temperature (°C)	−0.34	+0.25	1.16	0.79
	Air spec hum. (g kg^{-1})	3.61	+0.47	0.56	0.83
	Wind speed (m s^{-1})	5.643	−0.87	1.99	0.55
	Wind direction (°)	136.2	+11.72	27.52	0.40
	Surface albedo (−)	0.69	+0.05	0.07	0.62

Table 6 Simulated surface mass balance components in the different model mass balance zones for the reference experiment and the constant 0.8 albedo sensitivity experiment

Area	Variable	Reference experiment	Albedo sens. experiment	Relative change (%)
Ablation zone	Mass balance change	−703.6	−109.6	−84.42
	Net melt	−958.4	−365.1	−62.91
	Sublimation	−26.7	−22.8	−14.61
	Rainfall	112.9	106.7	−5.49
	Snowfall	168.6	171.6	−1.78
Percolation zone	Mass balance change	272.4	270.9	−0.55
	Net melt	−5.0	−4.5	−10.00
	Sublimation	−24.9	−22.4	−10.04
	Rainfall	21.7	20.9	−3.69
	Snowfall	280.6	276.9	−1.32
Dry snow zone	Mass balance change	130.12	127.22	−2.23
	Net melt	0.00	0.00	0.00
	Sublimation	−10.00	−9.60	−4.00
	Rainfall	1.72	1.68	−2.33
	Snowfall	138.40	135.10	−2.38
Whole ice sheet	Mass balance change	121.5	176.1	44.94
	Net melt	−93.5	−37.0	−60.43
	Sublimation	−19.2	−17.2	−10.42
	Rainfall	22.2	21.2	−4.50
	Snowfall	212.0	209.1	−1.37

The absolute mass balance terms are expressed in mmWE. Negative numbers indicate mass losses. Net melt is the amount of melt adjusted for retention of meltwater inside the snow pack and eventually refreezing. The relative changes are calculated as [(2)–(1)]/(1) with (1) the reference figures and (2) the constant 0.8 albedo results

simulation, this height is reduced to 61 cm in the reference experiment while it is 50% higher (91 cm) in the albedo sensitivity experiment. The impact is even larger at GIMEX-M6 situated in the ablation zone characterized by low albedo values. At GIMEX-M6, the appearance of ice at the surface is simulated on 8 July in the reference experiment with the melt of an additional 130 cm of ice afterwards. At the end of the constant 0.8 albedo experiment, the winter snow pack at GIMEX-M6 is not even completely melted away and 17 cm of snow remains above the ice at the end of August.

On average over the ice sheet (Table 6), melt decreases by more than 60% in the constant albedo simulation compared to the reference experiment. The other mass balance components only change in a minor way except the evaporative mass loss, which decreases by 10–15% in the model ablation and percolation zone. Therefore, the use of a constant 0.8 albedo has little impact on the simulation of the atmospheric variables but will lead to a significant underestimation of the modelled melt. In the perspective of mass balance calculations, this is of capital importance.

3.3 Model evaluation in the high dry snow zone (Summit)

AWS-Klinck is situated in the neighborhood of the Greenland ice-sheet summit. The simulated temperature is in agreement with observations during the day but is underestimated during the night when the temperature is below −25°C (Fig. 8). This leads to a negative temperature bias of about 3°C (Table 7). Part of the negative bias can be explained by the katabatic temperature inversion and the difference in height between the model's first level and the height of the measurements. Indeed, the measurements were taken at a height of 3 m above the surface while the model's lowest level is situ-

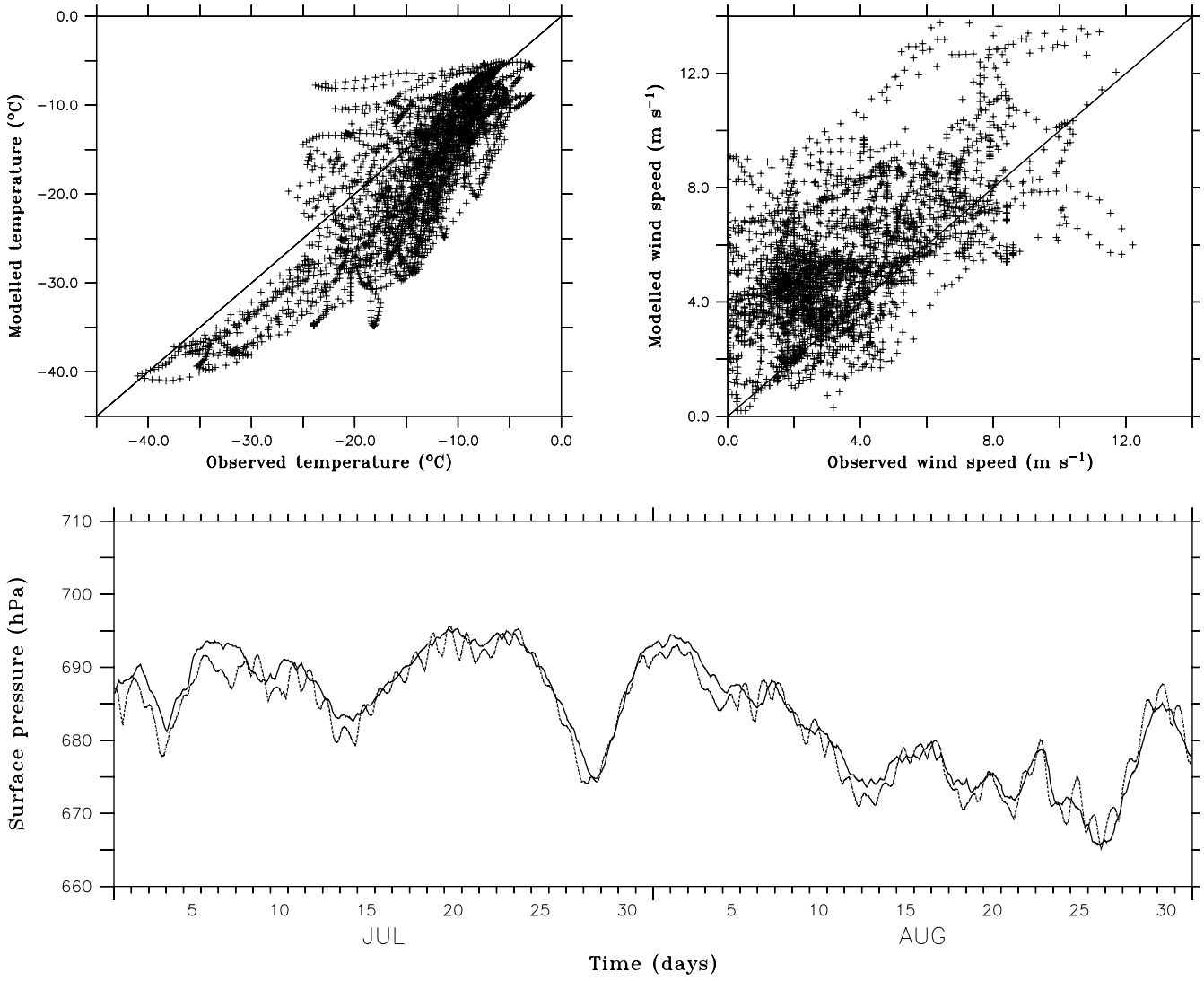

Fig. 8 MAR (*solid*) and observed (*dashed*) air temperature, wind speed and surface pressure at AWS-Klinck, which is located close to the ice-sheet summit

Table 7 Statistics at AWS-Klinck and Kangerlussuaq during the summer of 1991 based on 6-hourly values. The large MAR surface pressure bias and rmse at Kangerlussuaq is caused by the 290 m difference in surface height (Table 2)

Station	Variable	Obs mean	MAR bias	MAR rmse	MAR corr
AWS-Klinck (1st May ↔ 31st August)	Air temperature (°C)	−15.66	−3.12	5.12	0.87
	Wind speed (m s^{-1})	4.08	+1.8	2.64	0.72
	Wind direction (°)	164.8	+12.87	55.73	0.62
	Surface pressure (hPa)	683.10	+0.91	1.98	0.98
Kangerlussuaq (1st May ↔ 31st August)	Air temperature (°C)	7.52	−4.74	7.08	0.78
	Relative humidity (%)	65.13	+11.06	23.80	0.30
	Wind speed (m s^{-1})	3.64	−0.82	2.27	0.19
	Surface pressure (hPa)	1008.0	−40.48	40.36	0.98

ated at less than 1.5 m above the surface. In fact, due to the elevated surface height of AWS-Klinck, the lowest model level (pressure levels), which at mean sea level is normally situated at 2 m above the surface, is situated at 1.5 m above the surface near the summit of the Greenland ice sheet. Secondly, as already explained during the discussion of the results at ETH-Camp, Morcrette (2002) has shown that the radiative model used in MAR (as well as in the ERA-15 re-analysis) underestimates the downward infrared radiation for cold clear-sky situa-

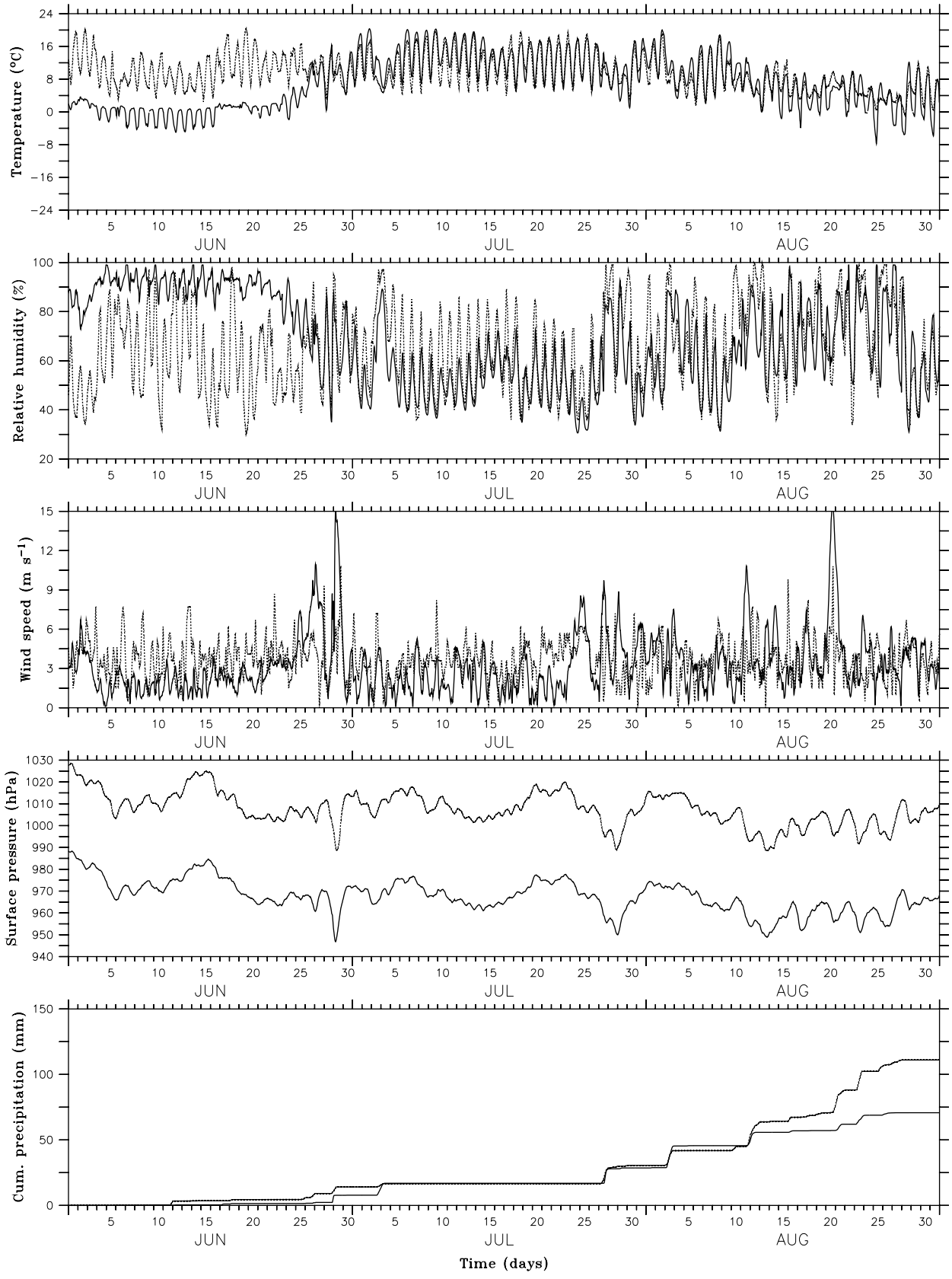

Fig. 9 MAR (*solid*) and observed (*dotted*) air temperature, relative humidity, wind speed, surface pressure and cumulative precipitation at Kangerlussuaq

tions. This is responsible for an underestimation of the air temperature, especially at the top of the ice-sheet where cold clear-sky situations dominate. Again, the accuracy of the radiation physics in polar conditions needs further improvement.

3.4 Model evaluation at Kangerlussuaq

At the start of the simulation, the tundra area near Kangerlussuaq is covered with snow which, explains why simulated air temperatures do not rise above 0°C. However, when all snow has melted away in the model, simulated temperatures agree very well with the observed ones (Fig. 9 and Table 7), stressing the need for correct initial conditions for the simulation of the summer climate.

In this context, it is also worth mentioning the results of Denby (2001), who found an important sensitivity of the simulated turbulent and longwave heat fluxes in the ice-sheet ablation zone, depending on the state of the tundra (snow covered or not).

The large surface pressure bias is caused by the difference in surface height (see Table 2). The resolution used is clearly not yet sufficient to take explicitly into account the narrow fjords which runs from the sea towards the ice-sheet margins through the tundra area.

Finally, MAR modelled precipitation corresponds closely with the observations until mid-August (lower graph in Fig. 9). Thereafter, about four precipitation events are simulated by MAR at the right moment but with a too-low intensity. The precipitation bias can be due to very localized orographic effects in the Kangerlussuaq fjord.

4 Conclusions and perspectives

A coupled atmosphere–snow regional climate model (MAR) applied over south Greenland with a high horizontal resolution of 20 km has been nested into ECMWF ERA-15 re-analysis. Lateral boundary conditions are updated every 6 h. Due to the coupling of the atmospheric model with the snow model, the snow albedo over the ice sheet is made dependent on the precipitated fresh snow. Inside the snow model, the history of the snow grain characteristics (sphericity, dendricity and grain size) is used to calculate the snow albedo.

The evaluation of the surface albedo simulation at ETH-Camp, GIMEX-M6 and GIMEX-M9 showed that an accurate surface albedo simulation, which is a requisite for a good surface mass balance simulation, strongly depends on the state of the snow pack at the start of the ablation season. Therefore, future high-resolution simulations of the Greenland surface mass balance by means of coupled atmosphere–snow models should not only focus on the summer season but also on the winter season. In that way, the initial conditions can be obtained more accurately. Moreover, close to the ice-sheet margin around the K-transect, the ice-sheet surface is found to be snow-free at the start of the simulation. Winter precipitation is not so important in this region, (Bromwich et al. 2001a) but certainly not equal to zero. On the other hand, the katabatic winds are very persistent and strong in this region which suggests that snow drifts take place. This, as well as the role of evaporation and sublimation, should be further investigated in the future.

Evaluation of the modelled surface radiative fluxes points to an overestimation of the solar downward radiative flux and an underestimation of the longwave radiative flux, although the simulated inter-daily variability due to cloud cover was mostly in agreement with the observations. The underestimation of the downward longwave radiative flux with the present version of the longwave scheme has been pointed out by Morcrette (2002) and will be corrected in the future by using an updated version of the radiative scheme. Also, the role of the microphysical parameterizations should be further investigated.

A sensitivity experiment in which the surface albedo was held constant at 0.8 over the whole ice sheet underlined the strong influence of this parameter on the simulation of the surface mass balance. This is particularly relevant in the model ablation zone where ice appears at the surface during the summer melting season. A constant 0.8 albedo weakly influences the atmospheric variables. However, on average over the ice sheet, there is 60% less melt. In the perspective of mass balance calculations, it is therefore of capital importance to use a variable albedo which evolves according to the state of the snow-ice surface.

The presented evaluation of the coupled atmosphere–snow Greenland climate model opens new perspectives in the study of the Greenland surface mass balance because of the coupling between the atmosphere and the snow model. In a next step, the model should be applied over the whole Greenland ice sheet and simulations covering longer time periods should be foreseen in order to study for example, the origins and mechanisms behind the inter-annual variability of the Greenland surface mass balance. Also, sublimation and the contribution of refreezing to the surface mass balance are topics that should be addressed with the present model.

Acknowledgements Filip Lefebre was financed by the Belgian Scientific Research Programme "Global Change and Sustainable Development (contract CG/10/09B)" of the Prime Minister's Science Policy Office, when writing this paper. We are very grateful to the Belgian Royal Meteorological Institute (KMI-IRM) for giving access to the European Centre for Medium-Range Weather Forecasts (ECMWF) data services. Dominique Lucas (ECMWF, Reading) is thanked for help with the ERA data. The authors would like to thank The Antarctic Meteorological Research Center, Space Science and Engineering Center, University of Wisconsin-Madison as well as the National Science Foundation for the AWS-Klinck data. Philippe Huybrechts (Vrije Universiteit Brussel, Brussels, Belgium) is thanked for kindly providing the Greenland

topography and land mask data. We gratefully acknowledge the Belgian Fonds de la Recherche Fondamentale Collective for providing computer facilities under project 2.4556.99 "Simulation numérique et traitement de données".

References

Ambach W (1988) Heat balance characteristics and ice ablation. Western EGIG-profile, Greenland. In: Thomsen T, Sögaard H, Braithwaite R (eds) Applied hydrology in the development of northern basins. Danish Society for Arctic Technology, Copenhagen, pp 59–70

Benson CS (1962) Stratigraphic studies in the snow and firn of the Greenland ice sheet. SIPRE(CRREL) Res Rep 70. CRREL, Hannover NH, 93 pp

Box J, Steffen K (2001) Sublimation on the Greenland ice sheet from automated weather station observations. J Geophys Res 106:33965–33982

Brasseur O, Gallée H, Creutin J-D, Lebel T, Marbaix P (2002) High resolution simulations of precipitations over the Alps with the perspective of coupling with a hydrological model. In: Beniston M (eds) Climate change: implications for the hydrological cycle and for water management. Advances in global change research, vol 10. Kluwer, Dordrecht, pp 75–100

van den Broeke MR, Duynkerke P, Oerlemans J (1994) The observed katabatic flow at the edge of the Greenland ice sheet during GIMEX-91. Global Planet Change 9:3–15

Bromwich D, Chen Q-S, Bai L, Cassano E, Li Y (2001a) Modeled precipitation variability over the Greenland ice sheet. J Geophys Res 106:33891–33908

Bromwich DH, Cassano JJ, Klein T, Heinemann G, Hines KM, Steffen K, Box JE (2001b) Mesoscale modeling of katabatic winds over Greenland with the Polar MM5. Mon Wea Rev 129(9):2290–2309

Brun E, David P, Sudul M, Brunot G (1992) A numerical model to simulate snowcover stratigraphy for operational avalanche forecasting. J Glaciol 38:13–22

Cassano J, Box J, Bromwich D, Li L, Steffen K (2001) Evaluation of Polar MM5 simulations of Greenland's atmospheric circulation. J Geophys Res 106:33867–33890

Davies H (1983) Limitations of some common lateral boundary schemes used in regional NWP models. Mon Wea Rev 111:1002–1012

Deardorff J (1978) Efficient prediction of ground surface temperature and moisture with inclusion of a layer of vegetation. J Geophys Res 83:1889–1903

Denby B (2001) Modelling and interpretation of turbulent fluxes in katabatic flows: applications to glaciers and the Greenland ice sheet. PhD thesis, Universiteit Utrecht

Ekholm S (1996) A full coverage, high-resolution, topographic model of Greenland computed from a variety of digital elevation data. J Geophys Res 101(B10):21961–21972

Forrer J, Rotach W (1997) On the turbulence structure in the stable boundary layer over the Greenland ice sheet. Bound Layer Meteorol 85:111–136

Gallée H (1995) Simulation of the mesocyclonic activity in the Ross Sea, Antarctica. Mon Wea Rev 123:2051–2069

Gallée H and Duynkerke P (1997) Air–snow interactions and the surface energy and mass balance over the melting zone of West Greenland during GIMEX. J Geophys Res 102:13813–13824

Gallée H, Schayes G (1994) Development of a three-dimensional meso-γ primitive equations model. Mon Wea Rev 122:671–685

Gallée H, Fontaine de Ghélin O, van den Broeke MR (1995) Simulation of atmospheric circulation during the GIMEX-91 experiment using a meso-γ primitive equations model. J Climate 8:2843–2859

Gallée H, Guyomarc'h G, Brun E (2001) Impact of snow drift on the Antarctic ice sheet surface mass balance: possible sensitivity to snow-surface properties. Bound Layer Meteorol 99 (1):1–19

Georgi F, Mearns L (1999) Regional climate modeling revisited. J Geophys Res 104:6335–6352

Gibson JK, Kållberg P, Uppala S, Hernandez A, Nomura A, Serrano E (1999) ERA-15 Description (Version 2—January 1999), ECMWF Re-analysis Project Report Series. European Centre for Medium-Range Weather Forecasts, Reading

Greuell W, Konzelmann T (1994) Numerical modelling of the energy balance and the englacial temperature of the Greenland ice sheet. Calculations for the ETH-Camp location (West Greenland, 1155 m a.s.l.). Global Planet Change 9:91–114

Hanna E, Valdes P (2001) Validation of ECMWF (re)analysis surface climate data, 1979–1998, for Greenland and implications for mass balance modelling of the ice sheet. Int J Climatol 21:171–195

Heinemann G (1999) The KABEG '97 field experiment: An aircraft-based study of katabatic wind dynamics over the Greenland ice sheet. Bound Layer Meteorol 93:75–116

Houghton J, Ding Y, Griggs D, Noguer M, van der Linden P, Dai X, Maskell K, Johnson C (eds) (2001) IPCC climate change 2001: the scientific basis. Contributions of working group I to the third assessment report of the intergovernmental panel on climate change. Cambridge University Press, Cambridge, 881 pp

Huybrechts P, Letréguilly A, Reeh N (1991) The Greenland ice sheet and greenhouse warming. Palaeogeogr Palaeoclim Palaeoecol 89:399–412

Key J, Wang X, Stroeve J, Fowler C (2001) Estimating the cloudy sky albedo of sea ice and snow from space. J Geophys Res 106:12489–12497

Lefebre F, Gallée H, van Ypersele JP, Greuell W (2003) Modelling of snow and ice melt at ETH-Camp (west Greenland): a study of surface albedo. J Geophys Res 108(D8):4231. DOI 10.1029/2001JD001160

Marbaix P (2000) A regional atmospheric model over Europe: adaptation for climate studies and validation. PhD thesis, Université catholique de Louvain, Louvain-la-Neuve

Marbaix P, Gallée H, Brasseur O, van Ypersele JP (2003) Lateral boundary conditions in regional climate models: a detailed study of the relaxation procedure. Mon Wea Rev 131(3):461–479

Morcrette J (1984) Sur la paramétrisation du rayonnement dans les modèles de la circulation générale atmosphérique. PhD thesis, Univ. des Sciences et Techniques de Lille, Lille

Morcrette J-J (2002) The surface downward longwave radiation in the ECMWF forecast system. J Climate 15:1875–1892

Morris E, Bader H-P, Weilenmann P (1997) Modelling temperature variations in polar snow using DAISY. J Glaciology 43(143):180–191

Naithani J, Gallée H, Schayes G (2002) Marine air intrusion into the Adelie land sector of East Antarctica—a study using Regional Climate Model (MAR). J Geophys Res 107(D11). DOI 10.1029/2000JD000274

Nolin A, Stroeve J (1997) The changing albedo of the Greenland ice sheet: implications for climate modelling. Ann Glaciol 25:51–57

Nomura A (1995) Global sea-ice concentration data set for use in the ECMWF re-analysis system. Technical Report 76. ECMWF, Shinfield Park

Oerlemans J, Vugts H (1993) A meteorological experiment in the melting zone of the Greenland ice sheet. Bull Am Meteorol Soc 74:355–365

Ohmura A, Steffen K, Blatter H, Greuell W, Rotach M, Stober M, Konzelmann T, Forrer J, Abe-Ouchi A, Steiger D, Niederbäumer G (1992) Energy and mass balance during the melt season at the equilibrium line altitude, Paakitsoq, Greenland ice sheet: progress report 2. Department of Geography, Swiss Federal Institute of Technology, Zürich

Ohmura A, Wild M, Bengtsson L (1996) A possible change in mass balance of Greenland and Antarctic ice sheets in the coming century. J Climate 9:2124–2135

Paterson W (1994) The physics of glaciers, 3rd edn. Pergamon/Elsevier Science Ltd

Pfeffer W, Meier M, Illangasekare T (1991) Retention of Greenland runoff by refreezing: implications for projected future sea level change. J Geophys Res 96:22117–22124

Reeh N (1991) Parameterization of melt rate and surface temperature on the Greenland ice sheet. Polarforschung, pp 113–128

Ritz C, Fabre A, Letréguilly A (1997) Sensitivity of a Greenland ice sheet model to ice flow and ablation parameters: consequences for the evolution through the last climatic cycle. Climate Dyn 13:11–24

Schytt V (1958) The inner structure of the ice shelf at Maudheim as shown by core drilling. Norwegian-British-Swedish Antarctic Expedition, 1949–52, Scientific Results 4, Glaciology 2. Norsk Polarinstitutt, Oslo, pp 115–151

Thomas RH, PARCA Investigators (2001) Program for arctic regional climate assessment (PARCA): Goals, key findings, and future directions. J Geophys Res 106(D24): 33691–33705

van de Wal R, Oerlemans J (1994) An energy balance model for the Greenland ice sheet. Global Planet Change 9:115–131